3-D RECONSTRUCTION OF DNA FILAMENTS FROM STEREO CRYO-ELECTRON MICROGRAPHS

Mathews Jacob, Thierry Blu and Michael Unser

Biomedical Imaging Group, DMT/IOA,
Swiss Federal Institute of Technology (EPFL),
CH-1015 Lausanne, SWITZERLAND
{Mathews.Jacob, Thierry.Blu, Michael.Unser}@epfl.ch

ABSTRACT

We propose an algorithm for the 3-D reconstruction of DNA filaments from a pair of stereo cryo-electron micrographs. The underlying principle is to specify a 3-D model of a filament – described as a spline curve – and to fit it to the 2-D data using a snake-like algorithm. To drive the snake, we constructed a ridge-enhancing vector field for each of the images based on the maximum output of a bank of rotating matched filters. The magnitude of the field gives a confidence measure for the presence of a filament and the phase indicates its direction. We also propose a fast algorithm to perform the matched filtering. The snake algorithm starts with an initial curve (input by the user) and evolves it so that its projections on the viewing plane are in maximal agreement with the corresponding vector fields.

1. INTRODUCTION

Cryo-microscopy is an approach that is used to image biomolecules such as DNA [1]. The technique uses a transmission electron microscope (TEM) to obtain stereo views of specimens preserved in vitrous ice. The TEM images provide the integrated density of the 3-D volume along the viewing direction. A typical stereo pair of micrographs is shown in Fig 1. In this paper, we address the problem of reconstructing the 3-D filament shape from such noisy stereo images. We can view the reconstruction process as composed of two separate problems: the detection of filament-like structures in the noisy 2-D images and the 3-D reconstruction given the detected filaments.

We solve the first problem using a directional matched filtering algorithm. We also develop an efficient implementation of the rotating filter analysis to construct a vector field (phase + magnitude) that will drive the 3-D reconstruction algorithm.
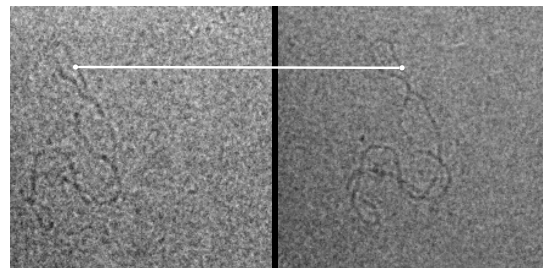
Fig. 1. Stereo views separated by $30°$ with a pair of corresponding points marked.

The 3-D reconstruction from the detected filaments is well defined once the correspondence between the detected points is known; it can be solved using simple geometrical considerations since the angle between the two views are known. Unfortunately, this correspondence is not known a-priori which makes the problem ill-posed. Morever, due to noise, a detected point in one image may not have a corresponding point detected in the other image.

To overcome these problems, we try to match the projections of a 3-D curve to the detected filaments. We start with an initial guess of the curve (based on the points specified by the user) which then the algorithm refines by putting it in correspondence with the data. This optimization is performed using a snake-like algorithm[2], where the external energy is a measure of the consistency between the curve projections and the detected filaments.

Our 3-D curve is described using cubic B-spline basis functions. Because of the minimum curvature property of cubic splines, there is no need for an explicit internal energy to constrain the smoothness of the curve [3]. The user interacts with the algorithm by initializing the curve and by introducing constraints; this information is incorporated into the model as external constraint energy. The algorithm is robust and precise because it performs a global optimization. This is in contrast with the more classical approaches such as morphological processing, flying cylinders [4] etc.

The paper is organized as follows. In section 2, we

present the ridge-enhancing vector field and its implementation. In section 3, we discuss the active contour algorithm and the various energies associated with it. In section 4, we explain the optimization scheme.

2. RIDGE-ENHANCING VECTOR FIELD

Matched filtering is a popular approach to detect signals in the presence of white Gaussian noise. It is optimal in the maximum likelihood sense. A matched filter detection of filament segments can be performed by using a collection of oriented filters $h_\theta(\mathbf{r}) = h(\mathbf{R}_\theta \mathbf{r})$, where $\mathbf{R}_\theta$ is a 2×2 rotation matrix. $h(\mathbf{r})$ is the typical profile of a horizontally-oriented filament. The most promising direction corresponds to the filter with the strongest output; the magnitude of the output reflects our confidence in the presence of a DNA filament at that location. This information can be encoded in a vector field $\mathbf{u}(\mathbf{r}) = u(\mathbf{r}) e^{j\theta^*(\mathbf{r})}$ whose direction and magnitude are given by

$$\theta^*(\mathbf{r}) = \arg\max_\theta \{(h_\theta * f)(\mathbf{r})\} \tag{1}$$

$$\mathbf{u}(\mathbf{r}) = \begin{cases} (h_{\theta^*} * f)(\mathbf{r}) & \text{if } (h_{\theta^*} * f)(\mathbf{r}) \geq 0 \\ 0 & \text{otherwise} \end{cases} \tag{2}$$

This rotating matched filter detection, although optimal, is computationally expensive and its precision is limited by the number of directions we consider. In the next subsection, we discuss an exact and computationally efficient implementation.

2.1. Rotating filters: Implementation

We restrict the class of filters to

$$h(\mathbf{r}) = \frac{\partial^2 g(\mathbf{r})}{\partial y^2} = \left. \frac{d^2}{d\alpha^2} g(\mathbf{r} + \alpha\, \mathbf{e}_y) \right|_{\alpha=0}, \tag{3}$$

where $\mathbf{e}_y$ is the vector $(0,1)$ and g is an isotropic window function; *i.e.*, $g(\mathbf{R}_\theta(\mathbf{r})) = g(\mathbf{r})$. We can show that this filter is steerable in the sense defined by Freeman and Adelson [5]. This leads to a fast implementation in terms of the Hessian matrix of $f * g$, denoted by

$$\mathbf{H}_{f*g} = \begin{bmatrix} \frac{\partial^2 f*g}{\partial x^2} & \frac{\partial^2 f*g}{\partial x \partial y} \\ \frac{\partial^2 f*g}{\partial x \partial y} & \frac{\partial^2 f*g}{\partial y^2} \end{bmatrix} \tag{4}$$

The implementation is given by the following proposition.

Proposition 1 *Let* $h(\mathbf{r}) = \frac{d^2 g(\mathbf{r})}{dy^2}$*, where g is an isotropic window function. Then, the ridge-enhancing vector field defined by* (1) *and* (2) *is given by*

$$\mathbf{u}(\mathbf{r}) = \begin{cases} \lambda_1(\mathbf{r})\, \mathbf{v}_2(\mathbf{r}) \,; & \text{if } \lambda_1(\mathbf{r}) \geq 0 \\ 0 & \text{otherwise} \end{cases} \tag{5}$$

where $\lambda_1(\mathbf{r})$ and $\mathbf{v}_2(\mathbf{r})$ are the maximum eigenvalue and the eigenvector corresponding to the minimum eigenvalue of $\mathbf{H}_{f*g}$ *respectively.*

Proof From the definition of h_θ, we have

$$\begin{aligned} h_\theta(\mathbf{r}) &= \left. \frac{d^2}{d\alpha^2} g(\mathbf{R}_\theta \mathbf{r} + \alpha\, \mathbf{e}_y) \right|_{\alpha=0} \\ &= \left. \frac{d^2}{d\alpha^2} g(\mathbf{r} + \alpha\, \mathbf{R}_\theta^{-1} \mathbf{e}_y) \right|_{\alpha=0} \end{aligned} \tag{6}$$

where we used the isotropy of g to get (6). Next, we express the second derivative along $\mathbf{w}_\theta = \mathbf{R}_\theta^{-1} \mathbf{e}_y$ in terms of the Hessian matrix;

$$h_\theta(\mathbf{r}) = \mathbf{w}_\theta^T \mathbf{H}_g(\mathbf{r}) \mathbf{w}_\theta \tag{7}$$

Using the commutativity of convolution and differential operators, we get

$$(h_\theta * f)(\mathbf{r}) = \mathbf{w}_\theta^T \mathbf{H}_{g*f}(\mathbf{r}) \mathbf{w}_\theta \tag{8}$$

Thus, the maximum eigenvector of $\mathbf{H}_{g*f}$ gives the direction along which $h_\theta * f$ is a maximum: $\mathbf{w}_{\theta^*} = \mathbf{v}_1$. Since the Hessian matrix is symmetric, the eigenvectors ($\mathbf{v}_1$ and $\mathbf{v}_2$) are orthogonal and we get (5).
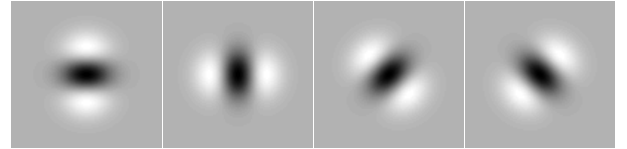

Fig. 2. Directional filters $h_\theta(\mathbf{r})$ for $\theta = 0$, $\theta = \frac{\pi}{2}$, $\theta = \frac{\pi}{4}$, $\theta = -\frac{\pi}{4}$

2.2. Choice of window function

We choose the window function to be a Gaussian for the following reasons:

1. Optimal profile for edges: Canny, in his seminal paper on edge detection [6], has derived the optimal operator for the detection of 1-D ridges in 1-D signals; this operator can be approximated closely with the second derivative of a Gaussian. For 2-D signals, the operator has to be applied orthogonal to the ridge, while smoothing along the ridge.

2. Separability: The Gaussian is the only function that is isotropic and separable at the same time. This results in fast implementation.

3. Localization: The Gaussian achieves the optimal compromise in terms of space-frequency localization (uncertainty principle).

Some filters h_θ for different values of θ are shown in Fig. 2. The result of the application of the ridge-enhancing algorithm to a cryo-electron micrograph containing DNA filaments is shown in Fig. 3. We see that it essentially detects the structure of interest although there is still some background noise.
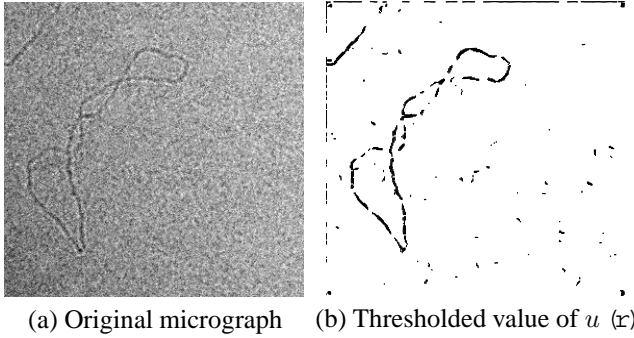

(a) Original micrograph   (b) Thresholded value of $u(r)$

Fig. 3. Illustration of the ability of the ridge-enhancing field to detect filaments.

3. 3-D RECONSTRUCTION

As discussed before, we have a curve model in 3-D that we refine to best fit the ridge-enhancing vector fields for both views. This algorithm is an adaptation of the classical active contour (snake) algorithm [2] with appropriate energies.

The curve description can be explicit [7, 2] or can be the level set of a surface. We resort to the former approach as the topology of the object remains the same and it is easy to introduce external constraints.

3.1. Parametric curve representation

A curve in 3-D space can be represented in terms of an arbitrary parameter t as $r(t) = (x(t), y(t), z(t))$. Such a parametric representation can be approximated efficiently by a linear combinations of shifted generating functions. If the curve is closed, the function vector $r(t)$ is periodic. Assuming the period M to be an integer, we describe the curve as

$$r(t) = \sum_{k=0}^{M-1} c_k \varphi_p(t-k), \qquad (9)$$

where

$$\varphi_p(t) = \sum_{k=-\infty}^{\infty} \varphi(t-kM) \qquad (10)$$

Here we have chosen $\varphi = \beta^3$ to be a cubic B-spline for the following reasons.

1. The parallel projection of a B-spline curve onto a plane is still a B-spline curve because the B-spline representation is invariant to affine transformations,

2. B-splines are compactly supported, which gives a local control over the contour.

3. Splines have excellent approximation properties

4. B-splines can be efficiently handled using filtering-based algorithms[8].

3.2. Internal energy

Conventional snakes are not parametric in the sense specified above. They are represented as an ordered collection of points. This is simple but requires the use of an explicit internal energy to enforce the smoothness and continuity of the curve. In contrast when the curve is represented in a cubic B-spline basis as in [7], this term is no longer required. This is due to the minimum curvature interpolation property of cubic spline curves [3], when described in the curvilinear abscissa. To ensure the validity of the assumption, we resample the initial curve (spline interpolation of the user input points) spacing the knots at equal intervals with respect to the curvilinear abscissa. The number of B-spline knots determines the internal energy of the curve. The absence of an explicit stiffness constraint also makes the optimization simpler.

3.3. External Energy

The choice of the external energy is the most crucial one; it is the term that drives the active contour close to the image features. As mentioned before, we project the 3-D curve onto the viewing planes; we choose the external energy as a measure of consistency between the curve projections and the ridge-enhancing field (5). Let the curve in 3-D be denoted by $\mathcal{C}$ and its projection along the kth viewing direction by $\mathcal{C}_k$. We denote the vector field corresponding to the kth view by u_k. Our measure of consistency between the curve projections and the detected filaments is

$$E = \sum_{k=0}^{1} \oint_{\mathcal{C}_k} |u_k(r) \cdot dr| \qquad (11)$$

One limitation of (11) is that it is computationally expensive, especially since it is to be evaluated over multiple iterations. Moreover, it gives a good measure only when the contour is close to the object (small region of attraction). Hence we also use an approximate, but fast, external energy to speed up the algorithm. It is given by

$$E = \sum_{k=0}^{1} \oint_{\mathcal{C}_k} (G_\beta * f_k)(r) \, dr, \qquad (12)$$

where f_k correspond to the kth image and G_β stands for a Gaussian of variance β. This energy has also a larger region of attraction, depending on the choice of β. We use this alternate energy for the initial optimization and switch to (11) at a later stage.

3.4. External Constraints

The more difficult cases can be handled by imposing some hard constraints. The user specifies any number of constraint points that are on the filament; we penalize the snake for not passing through them. This improves the robustness of the algorithm. The external constraint energy is given by

$$E_{\mathrm{const}} = \sum_{k=0}^{N-1} \left| \mathbf{r}\left(t_k\right) - \mathbf{r}_k \right|^2, \qquad (13)$$

where $\mathbf{r}_k$ is the kth constraint point and t_k is the associated parameter value.

4. USER INTERFACE

We have designed a user interface with two input modes.

1. Initialization mode: In this mode, the user enters corresponding points on the projective views. Once the curve is closed, we compute the corresponding 3-D curve by resampling the interpolated curve to a specified number of spline knots; this number determines the intrinsic stiffness of the snake.

2. Constraint Input mode: In this mode, the user can refine the curve by entering constraints. The curve computed in the initialization mode is further optimized with the new constraint points.

Fig. 4. Estimated 3-D shape of the molecule viewed from different angles. The curve is projected orthogonally to the corresponding viewing planes

5. OPTIMIZATION

We use a conjugate gradient optimization scheme. To reduce the computational cost and to improve the region of convergence, we adopt to a two-step strategy.

1. The cheap cost function (12) is used first. In this case, we also use a multiscale approach; we start with a large β followed by smaller values to speed up the iteration.

2. In the second step, we use the more precise cost function (11). The variance of the Gaussian window is a trade off between robustness to noise and precision; it depends on the width of the ridge and the noise variance.

Fig. 4 shows an example of the 3-D reconstruction of a DNA molecule obtained with our algorithm. The estimated 3-D curve is orthogonally projected onto different planes. The first projection corresponds to the view in Fig. 3-a.

6. CONCLUSION

We proposed a computational procedure for determining the 3-D shape of DNA filaments from stereo cryo-electron micrographs. We derived a ridge-enhancing vector field from the projections using rotating matched filters. The magnitude of the field gives the confidence measure of the presence of the filament; its phase gives the direction of the filament. We modelled the DNA filament as a cubic B-spline curve in 3-D and developed an active contour algorithm that finds the best match with the image data.

7. REFERENCES

[1] J. Dubochet, M. Adrian, I. Dustin, P. Furrer, and A. Stasiak, "Cryo-electron microscopy of DNA molecules in solution," *Methods Enzymol.*, pp. 507–518, 1992, .

[2] M. Kass, A. Witkin, and D. Terzopoulos, "Snakes:active contour models," *Int. J. Comp. Vision*, vol. 1, pp. 321–331, 1988.

[3] M. Jacob, T. Blu, and M. Unser, "A unifying approach and interface for spline-based snakes," in *Proc. SPIE Med. Imaging, Vol. 4322, San Diego*, 2001, pp. 340–347.

[4] F.P. Margalef, P. Furrer, M. Kunt, and J. Dubochet, "The flying cylinder: A new algorithm for filament recognition in noisy stereo images," *J. of Str. Biology*, 1995.

[5] W.T. Freeman and E.H. Adelson, "The design and use of steerable filters," *IEEE Trans. Pattern Anal. Mach. Intell.*, vol. 13, pp. 891–906, 1991, .

[6] J.F. Canny, "A computational approach to edge detection," *IEEE Trans. Pattern Anal. Mach. Intell.*, vol. 8, pp. 679–697, 1986.

[7] P. Brigger, J. Hoeg, and M. Unser, "B-spline snakes: a flexible tool for parametric contour detection," *IEEE Trans. Image Process.*, vol. 9, pp. 1484–1496, 2000.

[8] M. Unser, "Splines: a perfect fit for signal and image processing," *IEEE Signal Processing Magazine*, vol. 16, pp. 22–38, 1999.